Deformable Landmark-Free Active Appearance Models: Application to Segmentation of Multi-Institutional Prostate MRI Data

Robert Toth[1] and Anant Madabhushi[1]

Rutgers, The State University Of New Jersey. Piscataway, NJ, 08901, USA.

Abstract. Prostate segmentation is a necessary step for computer aided diagnosis systems, volume estimation, and treatment planning. The use of standard datasets is vital for comparing different segmentation algorithms, and 100 datasets from 4 institutions were gather to test different algorithms on T2-weighted MR imagery. In this paper, a landmark-free Active Appearance Model based segmentation algorithm was employed to segment the prostate from MR images. A deformable registration framework was created to register a new image to a trained appearance model, which was subsequently applied to the prostate shape to yield a final segmentation. Results on 50 training studies yielded a median Dice coefficient of 0.80, and the fully automated algorithm was able to segment each prostate in under 3 minutes.

1 Background and Motivation

Segmentation of the prostate boundary is useful for many applications, such as a computer aided cancer diagnosis systems [1], and treatment evaluation via planimetry-based volume estimation [2]. Several segmentation schemes for MR imagery of the prostate have been recently presented, including algorithms by Klein et al. [3], Martin et al. [4], Pasquier et al. [5], and Makni et al. [6]. Klein et al. [3] performed a registration between an MR image of the prostate and an atlas of training data to achieve a segmentation of the prostate. Martin et al. [4] also used an atlas of training images, but constrained the segmentation model through the use of a statistical shape model. Pasquier et al. [5] used an Active Shape Model [7] method for extracting a statistical shape model of the prostate, which then looked for strong gradients to identify the prostate edge. Finally, Makni et al. [6] used a statistical shape model of the prostate, and clustered the intensities within a manually placed region of interest into 3 clusters: surrounding tissues and fat, central prostate zone, and the peripheral prostate zone. Any pixels within the latter 2 zones were determined to be in the prostate.

In this paper, we similarly perform image registration to align the prostate in a new image to a collection of existing training images, but do so within an Active Appearance Model (AAM) framework [8,9]. With AAM's, Principal Component Analysis (PCA) is performed on the set of image intensities inside

the object of interest, as well as a parameterization of the shape, to generate a low dimensional appearance projection. Traditionally, to segment a new image, the projections are varied, and the original, high dimensional shape and appearance are reconstructed. In the algorithm used in this paper (based on [9]), a new image is deformably registered to the AAM. At each iteration of the registration, the high dimensional set of intensities are reconstructed, and the best intensity reconstruction is found. This registration is then applied to the prostate shape, to yield a segmentation of the prostate.

This algorithm is similar to the atlas-based approach [3], but instead of registering a new image to an atlas, the new image is registered to a statistical model of entire set of training data (defined using an AAM). While the original algorithm from which this is based [9] used an affine registration (scale, rotation, and translation) to register the new image to the AAM, this paper introduces a spline-based deformable registration component [10] to overcome differences in prostate shape and appearance due to highly varied multi-institutional data. These additional degrees of freedom are especially important when dealing with multi-institutional data (as in this dataset), because different acquisition protocols (such as the use, or lack of use, of the endorectal coil) can yield sub-par results when only linear (affine) transformations are considered. In addition, as in [9], a levelset representation of the shape to overcome issues associated with using landmarks such as triangulation errors and correspondence issues.

2 Methodology

2.1 Brief Overview

The algorithm used to segment the prostate in this challenge can be separated into two steps: (1) training, and (2) testing. The training step involves aligning the training images, and generating a levelset-based AAM. The testing step involves deformably registering a new image to the AAM and applying that registration to the shape to yield a final segmentation.

2.2 Notation

An image scene is defined as $\mathcal{C} = (C, f)$, where C represents a set of spatial locations, and each $c \in C$ represents a set of Cartesian coordinates $c = (x, y, z)$. The number of training images is denoted as N. The number of pixels in each image is denoted as $P = |C|$. The intensity at each $c \in C$ is denoted as $f(c)$ and the set of P intensities for training image i is denoted as F_i. A given training scene is denoted as $\mathcal{C}_n = (C_n, f_n)$. $C_n^{(in)} \subset C_n$ defines the set of pixels inside the prostate. A new image to be segmented is denoted as $\mathcal{C}_\theta = (C_\theta, f_\theta)$.

2.3 Training

1. Alignment. The prostate surfaces on all training images are first aligned using an affine transformation, to bring all the objects into the same coordinate frame.

2. Estimating Shape. To train the AAM, the prostate shape for training image $i \in \{1, \ldots, N\}$ is represented by the signed distances to the prostate surface [11], and is defined as, $L_i = \{l_i(1), \ldots, l_i(P)\}$, where

$$l_i(k) = \begin{cases} -\min\limits_{c \in C^{(In)}} \|c_k - c\|_2 & \text{if } c_k \in C_i^{(In)} \\ +\min\limits_{c \in C^{(In)}} \|c_k - c\|_2 & \text{if } c_k \notin C_i^{(In)}. \end{cases} \tag{1}$$

3. Principal Component Analysis. To generate the AAM, Principal Component Analysis (PCA) is performed on the set of N shapes $(L_1, \ldots, L_N)$, and N intensities $(F_1, \ldots F_N)$, which yields a matrix of eigenvectors ψ_L for the shape, and another matrix ψ_F for the intensities, as well as the mean shape and intensity values ($\overline{L}$ and $\overline{F}$, respectively). PCA is then used to project each training image's set of shapes and intensities into low dimensional spaces, defined as,

$$\hat{L} = \psi_L^{-1} \cdot (L - \overline{L}) \tag{2}$$

and

$$\hat{F} = \psi_F^{-1} \cdot (F - \overline{F}). \tag{3}$$

The shape and intensity projections are concatenated as $\hat{G} = [\hat{F}, \hat{L}]$, and a second PCA is performed on $\hat{G}_1, \ldots, \hat{G}_N$, resulting in a matrix of eigenvectors ψ_G, essentially linking the shape and intensity, as described in [8]. The first $|\hat{F}|$ rows of ψ_G represent the intensity projections, while the latter $|\hat{L}|$ rows of ψ_G represent the shape projections.

2.4 Testing

To segment a new study $\mathcal{C}_\theta$, registration is performed to fit the new image to the AAM. Let $T(F_\theta)$ represent the set of intensities, transformed by transformation T. The goal of the registration framework is to determine which transformation T should be applied to the new image to register it to the trained AAM. T is a general term which can represent any set of transformations, and in the experiments performed for these datasets, T represents linear (affine) transformations, as well as b-spline transformations [10]. To determine the cost of transformation T, the AAM is used to reconstruct the intensities, essentially determining how well the given intensities are represented in the training data.

The process to segment a new study $\mathcal{C}_\theta$ and yield the final segmentation $C_\theta^{(In)}$ is described as follows.

1. Calculate PCA Based Projection. Equation 3 is first used to calculate a low dimensional projection $\hat{F}_T$ of $T(F_\theta)$.

2. Reconstruct Linked Projections. Recall the the linked projections $\hat{G}$ represent a concatenation of both intensities and shape projections. Letting the first $|\hat{F}_T|$ rows of ψ_G, (representing the intensities) be denoted as $\psi_{G,F}$, the linked projections $\hat{G}_T$ (representing both intensity and shape) are reconstructed as,

$$\hat{G}_T = \psi_G \cdot \psi_{G,F}^{-1} \cdot \hat{F}_T. \tag{4}$$

3. Reconstruct Intensities and Shape. Given the linked projections $\hat{G}_T$, the original intensities and associated shape are next reconstructed. Letting $\hat{G}_T$ be defined as the concatenation of intensity and shape projections $\hat{G}_T = \left[\dot{F}_T, \dot{L}_T\right]$, the original P-dimensional intensities and shapes are reconstructed as,

$$R(F_T) = \overline{F} + \psi_F \cdot \dot{F}_T, \tag{5}$$

and

$$R(L_T) = \overline{L} + \psi_L \cdot \dot{L}_T. \tag{6}$$

Calculate Correlation. To evaluate how well a given transform T fits the image, the normalized cross correlation (NCC) is calculated between F_T and $R(F_T)$, denoted as $H_T = \mathrm{NCC}\left(F_T, R(F_T)\right)$.
Maximize Correlation. Since there now exists an evaluation of each transform T (denoted as H_T), T is varied until H_T is maximized, as

$$T^* = \arg\max_T H_T. \tag{7}$$

Then, the shape is calculated to yield a final segmentation as,

$$C_\theta^{(In)} = R(L_{T^*}) < 0. \tag{8}$$

While the original implementation [9] defined T as a linear transformation consisting of rotation, scale, and translation, in this study we performed a b-spline transformation following the linear registration. Hence the best linear transformation (maximizing H_T) was determined, after which a series of b-spline transformations were used to achieve a higher normalized cross correlation (H_T value) than linear transformations alone.

3 Experimental Design

3.1 Data Description

For this challenge, 100 datasets of T2-weighted prostate imagery from four different institutions were compiled, and randomized. The data consisted of both endorectal and non-endorectal data. 50 training studies with expertly annotated ground truth were made available for training, and 30 additional studies were provided (without any ground truth labels) to evaluate the algorithms.

3.2 Implementation and Efficiency

The algorithm described above was implemented in a completely automated fashion in C++ using the ITK framework. Table 1 contains additional implementation details. A genetic algorithm was used to solve Equation 8, and converged in under 180 seconds. To determine the accuracy of the algorithm on the training data, a leave-one-out experiment was performed, in which 49 studies were used to train, and 1 was used to test. The Dice similarity coefficient [12] was used to evaluate the accuracy.

4 Results and Discussion

The leave one out experiment resulted in a mean Dice coefficient of 0.79 and a median Dice coefficient of 0.80. The lower Dice values than those reported in [9] are most likely due to the variation in the training set from multiple institutions (such as the mix of endorectal and non-endorectal imagery) which can significantly change the prostate shape and appearance. While the use of a deformable registration algorithm was implemented to help alleviate that concern, future work will entail creating more patient-specific appearance models, rather than a global appearance model.

Qualitative results from the test data (in which no segmentations were given) are shown in Figure 1. It can be seen that the AAM was able to accurate detect the prostate boundary on the images shown, even though the appearance of the images vary greatly, especially in the use of the endorectal coil.

Table 1: Implementation and efficiency details.

	Parameter	**Value**
Algorithm	*Language:*	C++
	Compiler:	GCC 4.6
	Libraries/Packages:	ITK, OpenMP, Boost, Eigen
	GPU Optimizations:	None
	Multi-Threaded:	Yes
	User Interaction:	None (Fully Automated)
Machine	*CPU Clock Speed:*	2.67 GHz
	Machine CPU Count:	8
	Machine Memory:	32 GB
	Memory Used During Segmentation:	1.5 GB
Time	*Training Time:*	1 hour, 20 minutes (for 50 studies)
	Segmentation Time:	3 minutes (per study)
	User Interaction Time:	N/A

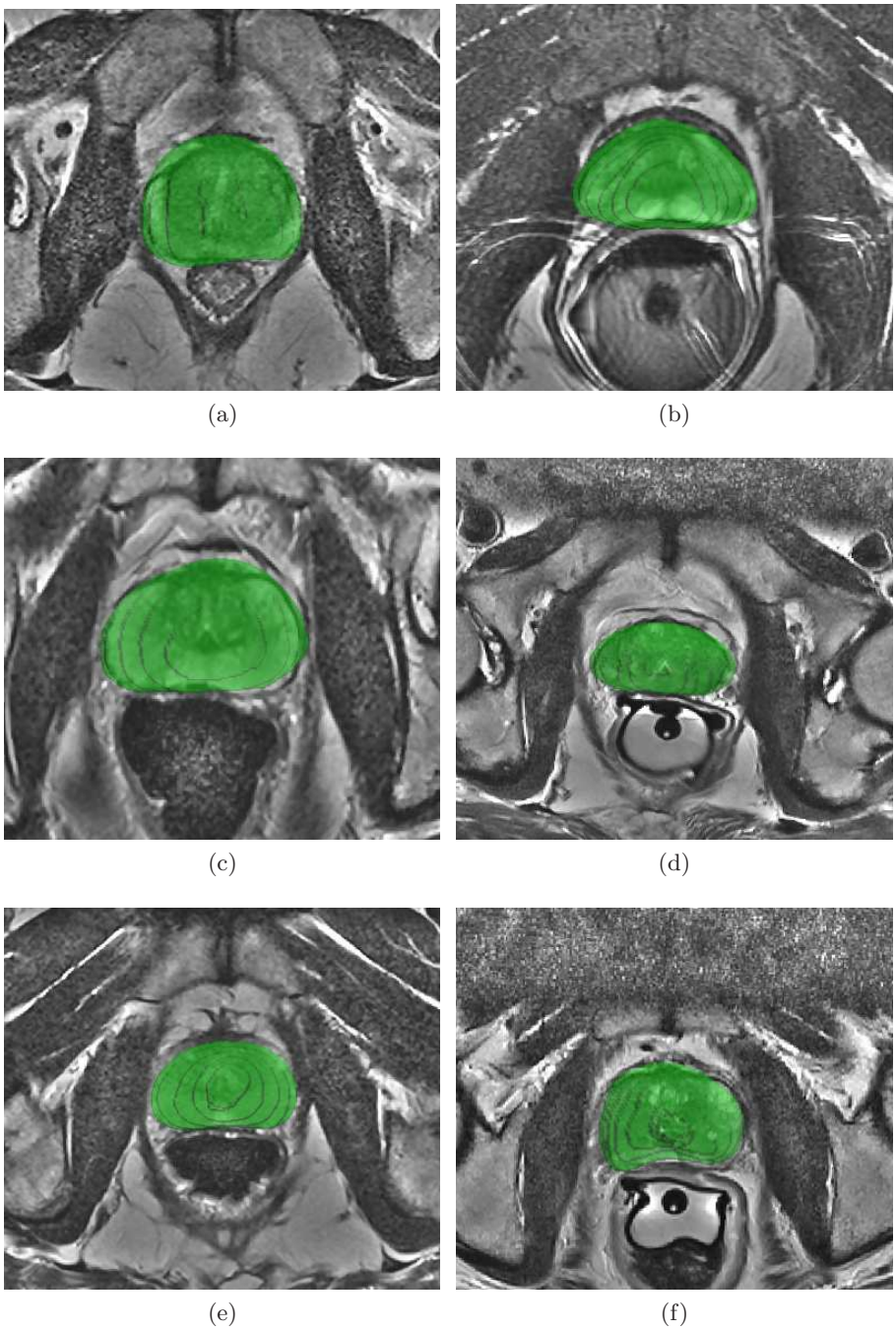

Fig. 1: Qualitative results from the segmentation challenge. In each case, the prostate segmentation volume is shown in green. Three of the cases are with an endorectal coil ((a), (c), (e)) and three are without ((b), (d), (f)).

5 Concluding Remarks

The data acquired for the prostate segmentation task was multi-institutional and therefore quite challenging to segment accurately. However, the use of the landmark-free Active Appearance Model based on a deformable registration framework was able to segment the training data with an accuracy of 0.80 and qualitatively able to segment the test data very well. Additional work will entail creating patient-specific, or institution-specific, appearance models to yield more accurate results.

Acknowledgments

This work was made possible via grants from the National Institute of Health (Grant Nos. R01CA136535-01, R01CA140772-01, R43EB015199-01, and R03CA143991-01).

References

1. Viswanath, S., Bloch, B., Genega, E., Rofsky, N., Lenkinski, R., Chappelow, J., Toth, R., Madabhushi, A.: A comprehensive segmentation registration and cancer detection scheme on 3 tesla in vivo prostate DCE MRI. Medical Image Computing and Computer Assisted Intervention **1** (2008) 662–669
2. Toth, R., Bloch, B., Genega, E., Rofsky, N., Lenkinski, R., Rosen, M., Madabhushi, A.: Accurate prostate volume estimation using active shape models on T2-weighted MRI. Academic Radiology **18**(2) (Jun 2011) 745–754
3. Klein, S., van der Heide, U., Lips, I., van Vulpen, M., Staring, M., Pluim, J.: Automatic segmentation of the prostate in 3D MR images by atlas matching using localized mutual information. Medical Physics **35**(4) (Apr. 2008) 1407–1417
4. Martin, S., Daanen, V., Troccaz, J.: Automated segmentation of the prostate in 3D MR images using a probabilistic atlas and a spatially constrained deformable model. Medical Physics **37**(4) (Apr 2010) 1579–1590
5. Pasquier, D., Lacornerie, T., Vermandel, M., Rousseau, J., Lartigau, E., Betrouni, N.: Automatic segmentation of pelvic structures from magnetic resonance images for prostate cancer radiotherapy. International Journal of Radiation Oncology and Biological Physics **68**(2) (2007) 592–600
6. Makni, N., Puech, P., Lopes, R., Dewalle, A.: Combining a deformable model and a probabilistic framework for an automatic 3D segmentation of prostate on MRI. International Journal of Computer Assisted Radiology and Surgery **4** (2009) 181–188
7. Cootes, T., Taylor, C., Cooper, D., Graham, J.: Active shape models - their training and application. Computer Vision and Image Understanding **61**(1) (Jan 1995) 38–59
8. Cootes, T., Edwards, G., Taylor, C.: Active appearance models. Pattern Analysis and Machine Intelligence, IEEE Transactions on **23**(6) (2001) 681–685
9. Toth, R., Madabhushi, A.: Multi-feature landmark-free active appearance models: Application to prostate mri segmentation. Medical Imaging, IEEE Transactions on **99** (2012)

10. de Boor, C.: A practical guide to splines. Springer-Verlag (1978)
11. Leventon, M., Grimson, W., Faugeras, O.: Statistical shape influence in geodesic active contours. In: Computer Vision and Pattern Recognition. Volume 1. (Jun 2000) 316–323
12. Dice, L.: Measures of the amount of ecologic association between species. Ecology **263** (1945) 297–302